Journal of Organometallic Chemistry, 300 (1986) 139–166
Elsevier Sequoia S.A., Lausanne – Printed in The Netherlands

ELECTRON TRANSFER AND TRANSIENT RADICALS IN ORGANOMETALLIC CHEMISTRY

JAY K. KOCHI

Department of Chemistry, University of Houston, University Park, Houston, Texas 77004 (U.S.A.)

(Received August 27th, 1985)

Summary

The variety of reactions available with metal carbonyls, both as mononuclear species and polynuclear clusters, is used to underscore the importance of electron transfer, transient radicals and ion radicals in organometallic chemistry.

The conceptual thinking in contemporary organometallic chemistry I believe reflects its mixed heritage. On one hand organic chemistry comfortably accommodates such transient or reactive intermediates as carbonium ions, free radicals, carbenes, etc., which are not isolable yet form an integral part of synthetic organic strategy. Stable structures, however bizarre, once they are established by X-ray crystallography, represent the foundations of inorganic chemistry. Stated alternatively, the pursuit of reactions is the principal concern in organic chemistry whereas inorganic chemistry is largely oriented toward structures, as also judged by the coverage of each subject in introductory textbooks [1]. The basic difference between the two lies in a kinetics approach as opposed to a thermodynamics approach to chemistry. This dichotomy is epitomized in organometallic chemistry and homogeneous catalysis in no better way than by the 16 and 18 electron rule [2], which is widely held and consistently applied [3]. One of its basic tenets applicable to dynamic processes states [2]: "Organometallic reactions, including catalytic ones, proceed by elementary steps involving only intermediates with 16 or 18 valence electrons".

Such a rule stems from the concept of 16 and 18 electron species as lying at energy minima along the reaction coordinate. However in reaction dynamics, the activation process must concern itself with structures at energy maxima.

Accordingly, my own thinking about organometallic reactions and catalysis has proceeded from quite a different perspective. Thus in an organometallic reaction, if a species has a stable 16 or 18 electron configuration it is unlikely to be an intermediate. In catalysis, if it can be isolated it is unlikely to be the catalytically active species.

0022-328X/86/$03.50

When I began to organize in my mind the myriad of wonderful new reactions in organometallic chemistry, I quickly rejected the traditional approach based on the 16 and 18 electron rule. Instead, I returned to the long forgotten, classical views on oxidation espoused by Michaelis which had fallen into disfavor [4]. (Perhaps rightly so, since he suggested that all oxidations proceeded by successive 1-electron steps via intermediate radicals.) Nonetheless the germ of Michaelis' ideas was credible, I thought. Accordingly, "Organometallic Mechanisms and Catalysis" was written in 1977 with a strong emphasis on 1-electron processes and odd-electron species such as radicals as well as radical ions in mind [5]. Despite the explosive development of organometallic chemistry and catalysis in the ensuing 9 years, the accretion of new knowledge has not caused me to wonder whether I should have taken a different tack. Quite the contrary, I perceive an increasing awareness of the role of electron transfer and the importance of transient radicals and radical ions in organometallic chemistry.

I wish to take this opportunity to present studies from our laboratories on some basic reactions of metal carbonyls. We focus here on metal carbonyls, since they are among the oldest organometals and their reactions are among the most fundamental processes in organometallic chemistry.

Ligand substitution of metal carbonyls

Extensive mechanistic studies have been carried out on the ligand substitution of a variety of metal carbonyl systems, and they are commonly considered to proceed via the even numbered, 16- and 18-electron intermediates [6]. Thus the displacements of ligands from a series of Group 6B metal carbonyls $LM(CO)_5$ by nucleophiles such as phosphines and arsines **N** have been reported to involve competitive dissociative (S_N1) and associative (S_N2) pathways, as summarized in Scheme 1. Nitrogen-centered ligands L which serve as σ donors are particularly good leaving groups. Consequently, such derivatives are versatile synthetic precursors.

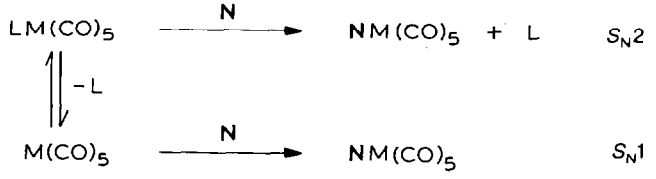

SCHEME 1

As recently as 5 years ago, three research groups independently discovered a much more facile process for ligand substitution. Thus Rieger and coworkers found that a rapid ligand substitution of the tricobalt cluster $PhCCo_3(CO)_9$ occurred when a small cathodic current [+e] was passed through the solution [7], e.g.:

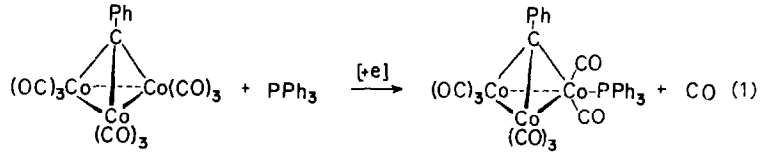

Robert Klingler working in my laboratory discovered that the tris-acetonitrile

complex *fac*-$(MeCN)_3W(CO)_3$ spontaneously underwent rapid ligand substitution of triphenylphosphine when a small anodic current [−e] was passed through the solution [8], i.e.:

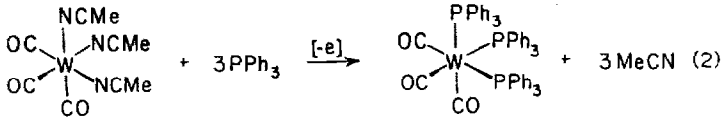

Wrighton and coworkers reported that a similar process could be induced photochemically [9], i.e.:

$$(MeCN)Re(CO)_3phen^+ + PPh_3 \xrightarrow{h\nu} (PPh_3)Re(CO)_3phen^+ + MeCN \qquad (3)$$

In each case the conventional thermal processes, the mechanisms of which are presumably depicted in Scheme 1, were too slow to compete.

The three ligand substitutions illustrated by eqs. 1, 2, and 3 have in common the corresponding radicals of the metal carbonyls as the key reactive intermediates. The anion and cation radicals (designated as $LM^{\cdot-}$ and $LM^{\cdot+}$ for simplicity) in eqs. 1 and 2, respectively, participate in basically the same chain mechanism, the propagation cycle of which consists of two sequential steps, viz., (a) ligand substitution and (b) electron transfer as shown below:

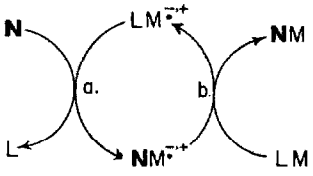

The rapid turnover of this catalytic cycle requires the 19- or 17-electron reactant ion radical ($LM^{\cdot-,+}$) to undergo rapid ligand substitution (step a) followed by efficient electron transfer of the product ion radical ($NM^{\cdot-,+}$) to regenerate the reactant ion radical (step b). Similarly the neutral 19-electron Re^0 intermediate in eq. 3 undergoes rapid ligand substitution (step a) followed by electron transfer with the cationic Re^I reactant to regenerate the Re^0 radical (step b). Accordingly this type of propagation cycle may be referred to as an electron-transfer chain or ETC catalysis.

Inhibition of ligand substitution by ETC catalysis occurs when either the reactant or product radical is diverted, either by self decomposition or reaction with a contaminant. The latter is often adventitious air (dioxygen) or traces of the by-products of degradation or synthesis. It is thus possible that a number of the substitution reactions which have been considered heretofore as proceeding via 16- or 18-electron intermediates may actually be inhibited forms of chain processes.

The initiation of the chain process requires either the oxidation of the metal carbonyl ($LM \xrightarrow{[-e]} LM^{\cdot+}$) or its reduction ($LM \xrightarrow{[+e]} LM^{\cdot-}$, $LM^+ \xrightarrow{[+e]} LM^{\cdot}$) which can be induced by either chemical oxidants and reductants, electrochemically, or photochemically. Among these modes of initiation, the electrochemical methods are the most versatile since they provide an infinitely variable access to redox changes. In the following, we wish to describe how electrochemical methods can be used to study ETC catalysis.

Let us consider the ligand substitution of the carbonylmanganese derivatives (η^5-MeCp)Mn(CO)$_2$L, hereafter referred to simply as MnL [10]. For the thermal process in this system, temperatures in excess of 200°C are said to be required to replace CO in the related (η^5-Cp)Mn(CO)$_3$ with a phosphine or arsine nucleophile [11]. We have observed a similar inactivity in the ordinary thermal substitution of the ligand from (η^5-MeCp)Mn(CO)$_2$L. Thus the replacement of pyridine by the phosphine in eq. 4 proceeds only upon refluxing a toluene solution overnight.

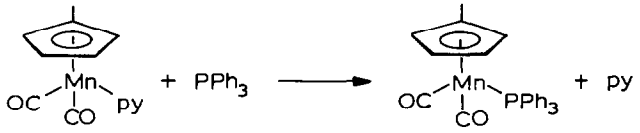

(4)

At a lower temperature (65°C), Mn(py) is recovered quantitatively after 4 h. By contrast, the stimulus provided only an electrical current leads to an efficient ligand substitution at much lower temperatures. Thus the phosphine substitution of Mn(NCMe) is complete at 22°C within 12 min, if a mere trickle of electrical current is passed through the acetonitrile solution (containing 0.1 *M* tetraethylammonium perchlorate TEAP as supporting electrolyte) with the aid of a set of platinum electrodes. Electrocatalysis is readily deduced by coulometry during the bulk electrolysis carried out at either constant potential or at constant current. From the measurement of the amount of charge (Faradays) passed through the solution, a current efficiency in excess of 290 equivalents Mn(Py) is obtained per electron. A catalytic cycle with a long kinetic chain length is thus indicated for this electrochemical process. The rate of ligand substitution under electrostimulation is visually apparent by the color change from orange of Mn(py) to the faint yellow color of the product. It can be followed quantitatively by monitoring the carbonyl bands by infrared spectrophotometry of both the reactant (ν(CO) of Mn(py), 1934, 1868 cm^{-1}) as well as the product (ν(CO) of Mn(PPh$_3$), 1884, 1944 cm^{-1}).

The course of ligand substitution can also be followed electrochemically by periodically monitoring the electrode potential during a run carried out at constant current. For example, the starting potential of −0.13 V vs. saturated NaCl SCE at the platinum gauze anode shown in Fig. 1 reflects the oxidation of Mn(py) [12]. The consumption of Mn(py) is accompanied by a gradual increase in the electrode potential until that time (t 12 min) at which there is a sharp rise in potential owing to the complete disappearance of Mn(py). The attainment of the new plateau at 0.28 V heralds the anodic oxidation of the product, which can be confirmed by examining the electrode potential of a fresh solution of Mn(PPh$_3$) under equivalent conditions.

The electrocatalytic procedure for substitution allows a variety of ligands **N** to be readily incorporated into the manganese carbonyl moiety. For example, starting with either the acetonitrile or the pyridine complex Mn(NCCH$_3$) or Mn(py), the various alkyl and arylphosphines and phosphites **N** listed in Table 1 partake in electrocatalytic substitutions with high current efficiencies:

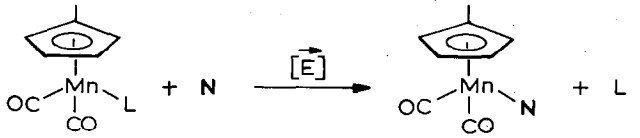

(5)

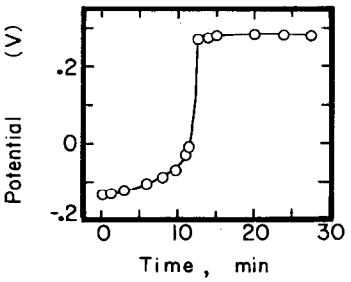

Fig. 1. Variation in the electrode potential during the electrocatalytic substitution of 4.0×10^{-2} *M* $MeCpMn(CO)_2py$ with 4.0×10^{-2} *M* PPh_3 in MeCN solution containing 0.1 *M* TEAP at a controlled current of 100 μA at 22°C.

Arsines and stibines as well as alkyl isocyanides are also efficiently incorporated. For each pair of reactants in Table 1, the appropriate control experiment performed in the absence of an anodic current ensures that the background, thermal reaction is unimportant. Indeed the solutions are initially prereduced under a nitrogen or argon atmosphere at a negative potential, typically -0.5 V at which none of the components is electroactive, to preclude adventitious (oxidized) impurities from catalyzing the thermal process. Under these conditions, none of the substitutions proceed at room temperature in the absence of electrostimulation.

The effectiveness of electrocatalytic substitution can be judged in two ways. First, the last column in Table 1 lists the current efficiency as measured by the reciprocal of the total charge *n* (Faraday) passed through the solution per mole *m* of starting material. As such, it represents a minimum value of the catalytic efficiency, or equivalently, the kinetic chain length of the radical process. The efficiency is dependent on both the nature of the displaced and substituting ligands L and N, as well as the bulk concentration of N. For example, the current efficiency for the replacement of acetonitrile in Mn(NCMe) is 3 times greater than pyridine substitution in Mn(py) and dimethyl sulfoxide substitution in Mn(DMSO), and more than 150 times greater than norbornylene substitution in Mn(NB) when PPh_3 is used as the common nucleophile under standard reaction conditions. Electrocatalytic substitution by added phosphines is more effective than that by phosphites. Thus the current efficiency for the electrocatalysis of Mn(NCMe) by the added nucleophiles PPh_3 and $P(OMe)Ph_2$ is exceedingly high ($> 10^3$), despite their presence in only equimolar amounts. Under equivalent conditions, the current efficiency for the utilization of the weaker $P(OPh)_3$ is only ~ 30. Moreover when the concentration of $P(OPh)_3$ is increased 10-fold the current efficiency rises to > 140.

Acetonitrile is a considerable more effective solvent than acetone for electrocatalytic substitution in this series of manganese carbonyls. Thus the current efficiencies in acetonitrile are higher by a factor of more than 10 relative to those carried out in acetone. Furthermore, acetonitrile is an effective solvent for substitution even when it is present as a ligand to be displaced in the complex Mn(NCMe). Likewise, tetrahydrofuran can be used as the solvent for the substitution of Mn(THF) with triphenylphosphine, pyridine, and acetonitrile.

In order to probe the origin of the electrocatalysis in ligand substitution, we examined the transient electrochemical behavior of the manganese carbonyls in Table 1, both in the absence and presence of added nucleophiles N. The cyclic

TABLE 1

ELECTROCATALYSIS OF THE LIGAND EXCHANGE OF VARIOUS MANGANESE CARBONYL DERIVATIVES MnL BY ADDED NUCLEOPHILES N [a]

MnL (mmol)	N (mmol)	Solvent	Current (μA)	$\frac{m}{n}$ [b]
MeCN (0.48)	PPh_3 (0.48)	MeCN	100	1013
MeCN (0.48)	$CNCMe_3$ (0.48)	MeCN	100	365
MeCN (0.31)	$P(Me)Ph_2$ (0.40)	MeCN	50	1004
MeCN (0.19)	$P(C_6H_4Me\text{-}p)_3$ (0.20)	MeCN	50	748
MeCN (0.16)	$P(C_6H_4Cl\text{-}p)_3$ (0.20)	MeCN	50	139
MeCN (0.12)	$P(OMe)Ph_2$ (0.14)	MeCN	100	833
MeCN (0.13)	$P(OPh)_3$ (0.15)	MeCN	100	29
MeCN (0.12)	$P(OPh_3)$ (1.9)	MeCN	100	142
MeCN (0.11)	$P(OMe)_3$ (0.13)	MeCN	100	196
MeCN (0.19)	$AsPh_3$ (0.21)	MeCN	100	82
MeCN (0.17)	$SbPh_3$ (0.20)	MeCN	200	96
py (0.076)	PPh_3 (1.5)	Me_2CO	50	92
py (0.048)	PPh_3 (0.48)	MeCN	100	291
py (0.012)	$CNCMe_3$ (0.15)	Me_2CO	100	64
py (0.10)	PEt_3 (0.12)	Me_2CO	100	174
py (0.10)	$P(OPh)_3$ (1.9)	Me_2CO	1000	5.2
THF (0.23)	PPh_3 (0.23)	THF	500	56
THF (0.23)	py (0.30)	THF	1000	91
Me_2SO (0.17)	PPh_3 (0.19)	MeCN	100	338
norbornene (0.094)	PPh_3 (0.095)	MeCN	1000	71

[a] Controlled-current oxidations at a Pt-gauze electrode performed at 22°C in 12 ml of solvent, and afforded quantitative yields of product, unless otherwise noted. In acetone and MeCN the supporting electrolyte was 0.1 *N* tetraethylammonium perchlorate (TEAP) and in THF, 0.1 *N* tetrabutylammonium perchlorate (TBAP) was employed. [b] The current efficiency, m/n, defined as the moles of starting material consumed divided by the Faradays of charge passed through the solution. All current efficiencies are reported for the conversion of all the starting material.

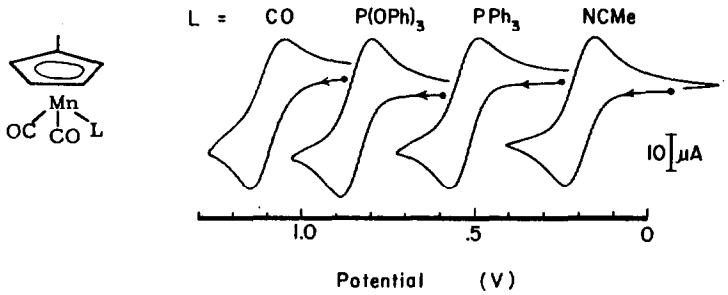

Fig. 2. Systematic variation in $E°$ for various manganese carbonyl derivatives MnL, as shown by the reversible cyclic voltammograms recorded at a sweep rate of 100 mV s^{-1} in acetonitrile containing 0.1 *M* TEAP at 22°C (except for Mn(CO) at −28°C and 200 mV s^{-1}). L from left to right: CO, $P(OPh)_3$, PPh_3, NCMe.

voltammetry (CV) was carried out at a stationary platinum microelectrode in acetonitrile, methylene chloride or acetone solutions containing 0.1 *M* tetraalkylammonium perchlorates as supporting electrolytes. The initial anodic scans for the cyclic votammograms of the pyridine, triphenylphosphine, and carbon monoxide derivatives of $MeCpMn(CO)_2L$ in Fig. 2 are all characterized by ratios of the anodic and cathodic currents (i_p^a/i_p^c) of unity and by anodic and cathodic peak separations ($E_p^a - E_p^c$) of near 60 mV for reversible one-electron processes, i.e.:

$$MeCpMn(CO)_2L \overset{E°}{\rightleftharpoons} MeCpMn(CO)_2L^+ + e^- \quad (6)$$

The magnitude of the reversible oxidation potentials $E°$ of the series of MnL listed in Table 2 is strongly dependent upon the nature of the coordinated ligand L. Thus the nitrogen-centered ligands such as amines and nitriles effect the most negative values in the range, $-0.04\ V < E° < 0.19\ V$. The reversible potentials of alkyl- and aryl-phosphine complexes are clustered around 0.5 ± 0.1 V, but those of corresponding phosphites are significantly more positive [13]. Among carbon-centered ligands, the values of $E°$ become progressively more positive in the order: alkene (norbornene, 0.44 V) < isocyanide (t-BuNC, 0.53 V) ≪ carbon monoxide (1.15 V). Indeed, the potential of the carbon monoxide complex $MeCpMn(CO)_3$ is the most positive of the derivatives listed in Table 2. We can deduce from these trends that the ease with which various MnL are oxidized is qualitatively dependent on the σ-donor property of L and by its π-acidity. For example, among complexes with nitrogen ligands, $E°$ becomes progressively more negative with increasing base strengths of L in the order: acetonitrile < pyridine ≪ piperidine. Moreover, we infer from the significantly more negative value of $E°$ for Mn(CNBu-t) compared to the $E°$ for Mn(CO) that the ligand π-acidities are in the order: carbon monoxide > t-butyl isocyanide.

The cyclic voltammetry of MnL in the presence of added nucleophile N provides unique insight into the mechanism of electrocatalysis. Thus Fig. 3 illustrates how the presence of triphenylphosphine leads to a drastic alteration of the well-behaved, reversible CV of Mn(NCMe). In particular the reactant wave (R = Mn(NCMe)) in Fig. 3b becomes clearly irreversible, as indicated by the absence of the coupled cathodic wave shown in Fig. 3a. Furthermore, the anodic peak current i_p^a for Mn(NCMe) decreases in magnitude in proportion to the concentration of PPh_3

TABLE 2

THE REVERSIBLE CV PARAMETERS OF VARIOUS MANGANESE CARBONYL DERIVATIVES MnL [a]

L	Solvent	$(E_p^{ox} + E_p^{red})/2$ (V)	$E°$ (V)	i_p^a/i_p^c
$HN(CH_2)_5$	Me_2CO	0.02	−0.04	1.1
NC_5H_5 (py)	Me_2CO	0.14	0.11	1.0
MeCN	Me_2CO	0.18	0.12	1.0
MeCN	CH_2Cl_2	0.20	0.15	1.0
MeCN	MeCN	0.22	0.19	1.0
PEt_3	Me_2CO	0.44	0.40	1.0
norbornene	MeCN	0.49	0.44	1.1
$P(Me)Ph_2$	MeCN	0.53	0.49	1.0
$P(C_6H_4Me\text{-}p)_3$	MeCN	0.53	0.50	1.0
PPh_3	MeCN	0.55	0.52	1.0
PPh_3	Me_2CO	0.55	0.52	1.0
$CNCMe_3$	MeCN	0.58	0.53	1.0
$CNCMe_3$	Me_2CO	0.59	0.54	1.0
$P(C_6H_5Cl\text{-}p)_3$	MeCN	0.64	0.60	1.0
$P(OMe)Ph_2$	MeCN	0.65	0.62	1.0
$P(OMe)_3$	MeCN	0.72	0.68	1.0
$P(OPh)_3$	MeCN	0.91	0.85	1.0
CO	MeCN	1.20	1.15	1.0

[a] Cyclic voltammetry performed at a Pt microelectrode with solutions 10^{-3} *M* in substrate and 0.1 *N* in supporting electrolyte (tetraethylammonium perchlorate for MeCN or acetone, tetrabutylammonium perchlorate for: THF of CH_2Cl_2). Unless otherwise noted, the scan rate was 100 mV s^{-1} and *T* 22°C. Potentials are reported relative to the Cp_2Fe/Cp_2Fe couple taken to have $(E_p^{ox} + E_p^{red})/2 = 0.31$ V in all solvents. [b] Scan rate 200 mV s^{-1}, *T* 55°C. [c] Scan rate 800 mV s^{-1}. [d] Scan rate 200 mV s^{-1}, *T* −50°C. [e] Scan rate 200 mV s^{-1}, *T* −28°C.

(compare Fig. 3b and 3c), and the diffusion current falls to near zero. This behavior requires that Mn(NCMe) be removed from the vicinity of the electrode by a process which is nonfaradaic i.e., one which does not require a net flow of current. Such a process simultaneously leads to the substitution product (P = $Mn(PPh_3)$), which is clearly in evidence in Fig. 3b and 3c by its reversible CV wave at the higher potential of $E°$ 0.55 V. In other words, the anodic electrode process leading to the depletion of Mn(NCMe) also results in the concomitant formation of $Mn(PPh_3)$. Since the electrode process at *E* 0.22 V is one in which the 17-electron cation $Mn(NCMe)^+$ is generated, it must be the species involved in the ligand exchange to afford the substitution product, i.e.:

$$Mn(NCMe)^+ + PPh_3 \rightarrow Mn(PPh_3)^+ + MeCN \quad (7)$$

Indeed the experiments to be described will demonstrate that the cation is significantly more reactive to phosphine substitution than its neutral, diamagnetic precursor Mn(NCMe).

Independent studies of the facile substitution of cations were carried out by the prior generation of $Mn(NCMe)^+$ as a deep orange solution. The bulk electrolysis of Mn(NCMe) in acetonitrile at a constant potential of +0.5 V required the passage of 1.0 Faraday of charge per mole of Mn(NCMe), i.e.:

$$Mn(NCMe) \xrightarrow{[\vec{E}]} Mn(NCMe)^+ + e \quad (8)$$

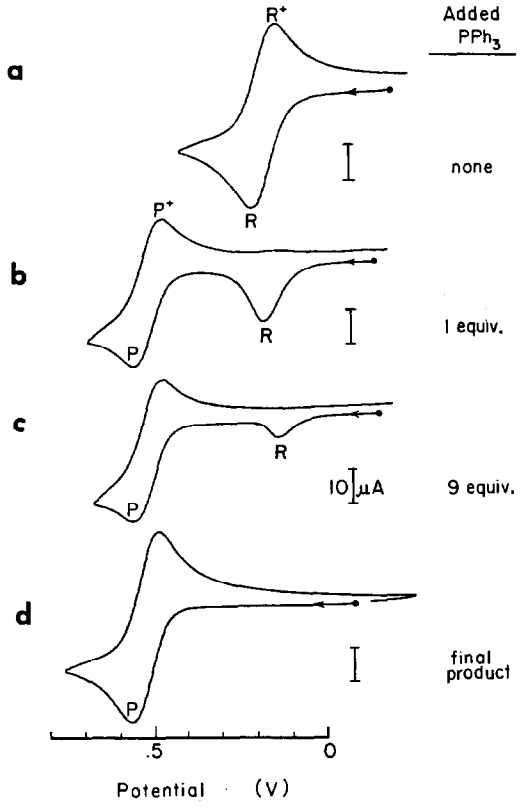

Fig. 3. The dramatic effect of added PPh_3 on the reversible CV of 1.0×10^{-3} *M* Mn(NCMe) in acetonitrile containing 0.1 *M* TEAP at a scan rate of 200 mV s^{-1} at 22°C. The CV waves of Mn(NCMe) R and $Mn(PPh_3)$ P are indicated for solutions containing (a) no, (b) one, and (c) nine equiv. of added PPh_3; (d) CV of authentic $Mn(PPh_3)$ under the same conditions.

Provided the temperature was not allowed to rise above −40°C, the re-reduction of $Mn(NCMe)^+$ could be effected quantitatively back to the neutral precursor, as shown by the cyclic voltammogram in Fig. 4b.

Addition of triphenyl phosphite to the solution of $Mn(NCMe)^+$ at −40°C immediately led to a deep orange-brown solution, which proved to contain only $Mn[P(OPh)_3]^+$, i.e.:

$$Mn(NCMe)^+ + P(OPh)_3 \xrightarrow[-40°C]{\text{fast}} MnP(OPh)_3{}^+ + MeCN \qquad (9)$$

as shown by the cyclic voltammogram in Fig. 4c. The same cationic product could be independently generated by the bulk electrolysis of $Mn[P(OPh)_3]$ at +1.0 V.

Similar results of facile cation substitution are obtained between triphenylphosphines and the pyridine analog $Mn(py)^+$, which is generated by the bulk electrolysis of Mn(py) in acetone at −30°C, i.e.:

$$Mn(py)^+ + PPh_3 \rightarrow Mn(PPh_3)^+ + py \qquad (10)$$

Bulk electrolysis of Mn(NCMe) and Mn(py) must be carried out at relatively low temperatures to minimize the decomposition of the labile cations $Mn(NCMe)^+$ and

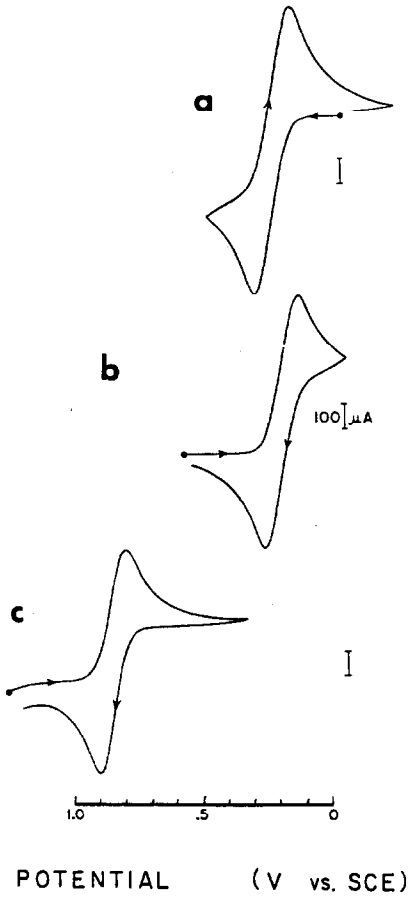

Fig. 4. (a) Reversible oxidation of Mn(NCMe) in acetonitrile containing 0.1 *M* TEAP at −35°C and a scan rate of 50 mV s^{-1}. (b) Reversible reduction of the solution in (a) after exhaustive oxidation of 0.5 V and −35°C. (c) Cyclic voltammogram (initial negative scan) of the solution in (b) immediately after the addition of excess $P(OPh)_3$.

$Mn(py)^+$, respectively. Consequently, it was not experimentally feasible to measure the rates of the cationic ligand substitutions described in eqs. 9 and 10 at the ambient temperatures employed in the electrocatalytic studies. Nonetheless, the facility with which such cationic substitutions occurs at temperatures below −30°C does provide unequivocal grounds for their participation in the electrocatalytic cycles. Electrocatalysis as described above implies the passage of current, however small, through the solution during ligand substitution. If the passage of an electrical current through a solution of Mn(NCMe) and PPh_3 is abruptly interrupted, the ligand substitution continues on for a substantial period of time. The latter indicates that the substitution reaction in eq. 11 can proceed at an appreciable rate even

$$Mn(NCMe) + PPh_3 \rightarrow Mn(PPh_3) + MeCN \qquad (11)$$

without a continual application of an electrode potential to the solution. To test this notion, we initially oxidized a very small portion (~ 2%) of Mn(NCMe) to the cation

$Mn(NCMe)^+$ at 0°C, and then disconnected the electrochemical circuit. Upon the addition of PPh_3, the visual change of the solution containing Mn(NCMe) to the color of $Mn(PPh_3)$ was apparent within 30 s. Moreover, the substitution product could be identified positively by its characteristic infrared spectrum in > 95% yield.

$$Mn(NCMe) + PPh_3 \xrightarrow{[2\%\ Mn(NCMe)^+]} Mn(PPh_3) + MeCN \quad (12)$$

Similarly, Mn(py) could be completely converted to the phosphine analog $Mn(PPh_3)$ be catalytic amounts of the cation $Mn(py)^+$, without the continued passage of current.

The ease with which the catalytic ligand substitution can be chemically initiated (as in eq. 12) depends on the reduction potential of MnL. Thus it may even be induced adventitiously when a readily oxidized manganese carbonyl such as Mn(NCMe) or Mn(py) is casually exposed to air.

Ligand substitution in its most general form represents an exchange process such as:

$$MnL + N \rightleftharpoons MnN + L \quad (13)$$

The notation Mn in eq. 13 designates the carbonylmanganese moiety (η^5-$C_5H_4Me)Mn(CO)_2$ and L and N represent the displaced and substituting ligands, respectively. Electrocatalysis of ligand substitution thus refers to the promotion of eq. 13 at an electrode with minimal consumption of current, under conditions in which the conventional thermal process is either nonexistent or unimportant. Since the electrochemically induced process is truly catalytic, the electrode only facilitates the rate of ligand substitution and does not alter the position of the equilibrium in eq. 13.

The well-behaved electrochemical characteristics of the series of manganese carbonyls MnL allow us to establish the kinetics and mechanism of electrocatalysis for the ligand substitution process in considerable, quantitative detail. We begin the discussion by emphasizing the high turnover numbers in excess of 1000 which can be achieved for electrocatalysis. As such, the chain substitution can be triggered by either a direct chemical (eq. 12) or an electrochemical (eq. 5) method of initiation. Indeed the anode provides a unique device for continuously generating the active species, which is readily identified by both transient and bulk electrochemical methods as the metastable 17-electron cation radical:

$$\textit{Initiation}: MnL \overset{[\vec{E}]}{\rightleftharpoons} MnL^+ + e \quad (14)$$

The propagation steps for the catalytic chain process stem from the enhanced rates of ligand substitution which we have established in eqs. 9 and 10 for such cations, i.e.:

$$\textit{Substitution}: MnL^+ + N \overset{k_1}{\rightleftharpoons} MnN^+ + L \quad (15)$$

The propagation sequence is completed by the electron transfer process in eq. 16:

$$\textit{Electron transfer}: MnN^+ + MnL \overset{k_2}{\rightleftharpoons} MnN + MnL^+ \quad (16)$$

Substitution and electron transfer in eqs. 15 and 16 together represent the

minimum number of discrete steps to constitute the catalytic cycle required for the overall stoichiometry in eq. 13. Such a chain mechanism for electrocatalysis is schematically represented in Scheme 2.

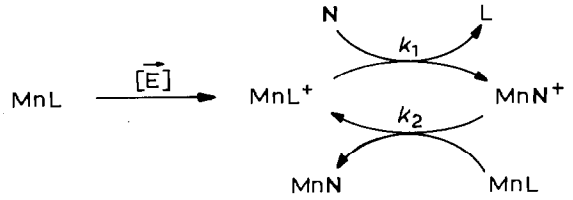

SCHEME 2

The formulation in Scheme 2 emphasizes the equivalence between the electrode mediated and the chemically induced methods for the initiation of the electrocatalysis. If substitution and electron transfer in eqs. 15 and 16 are both efficient, Scheme 2 predicts the occurrence of electrocatalytic processes with high turnover numbers. However, it is important to note that the reduction potential $E°$ of the product MnN^+ in eq. 15 is more positive than the potential $[E]$ at which the electrocatalysis is effectively initiated. Accordingly, it is also possible for the catalytic cycle to be completed by back electron transfer at the electrode potential $[E]$, i.e.:

$$MnN^+ + e \xrightarrow{[\vec{E}]} MnN \tag{17}$$

Under these circumstances, an alternative mechanism exists in which the electrocatalysis is strongly mediated by the electrode (Scheme 3). This electrocatalytic process will be particularly beneficial for those ligand substitutions with short kinetic chain lengths, since the current efficiency will not be critically dependent on the facility of the electron transfer step in eq. 16.

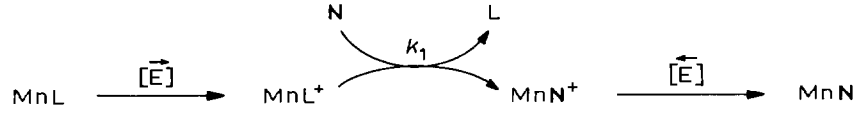

SCHEME 3

The essential difference between the mechanisms in Schemes 2 and 3 resides in the pathways by which electron transfer to the cationic product MnN^+ is effected. In Scheme 2, electron transfer by eq. 16 is a homogeneous process, whereas in Scheme 3 it occurs at an electrode surface (eq. 17). Since both processes are likely to be outersphere electron transfers, they are expected to be highly competitive. Indeed the partitioning between homogeneous and heterogeneous electron transfer represents a characteristic ambiguity in many electrochemical $\vec{E}C\vec{E}$ processes. Accordingly, let us consider the kinetics of electrocatalysis using the generalized Scheme 4 for the ECE process which is applicable to ligand substitution.

The kinetics for Scheme 4 can be immediately simplified by first focussing on the ligand substitution of Mn(NCMe) by PPh_3 in eq. 11. In this system, the ligand exchange step in eq. 18, as well as the electron transfer step in eq. 19, are both

$$Mn(NCMe)^+ + PPh_3 \rightarrow Mn(PPh_3)^+ + MeCN \tag{18}$$

$$Mn(PPh_3)^+ + Mn(NCMe) \rightarrow Mn(PPh_3) + Mn(NCMe)^+ \tag{19}$$

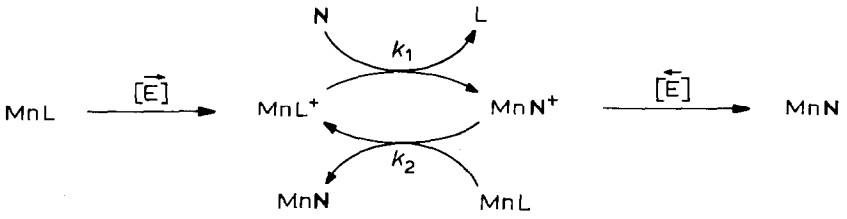

SCHEME 4

essentially irreversible: the first owing to the absence of the reverse step as shown by cyclic voltammetry, and the second arising from the large separation in the reduction potentials $E°$ for $Mn(NCMe)^+$ and $Mn(PPh_3)^+$ in Table 1.

Digital simulation of the cyclic voltammogram of Mn(NCMe) in the presence of added PPh_3 is carried out using the method of finite differences, as described by Feldberg [14]. Accurate simulation requires a knowledge of $E°$ for Mn(NCMe) and $Mn(PPh_3)$ as well as their intrinsic heterogeneous rate constants k_s and diffusion coefficients D, which can be determined independently. Thus our immediate goal is to substantiate the kinetic form of Scheme 4 and to determine the homogeneous kinetic parameters k_1 and k_2 in eqs. 15 and 16, respectively. Figure 5 (leftside) illustrates how the cyclic voltammogram of Mn(NCMe) is affected by the presence of PPh_3 at different CV sweep rates. The values of the rate constants k_1 and k_2 are determined by an iterative procedure, in which a value of k_2 is arbitrarily selected at first, and the value of k_1 varied until the match of the simulated and experimental cyclic voltammograms is optimized. The procedure is repeated until successful simulation is achieved with $k_1 = 1.3 \times 10^4\ M^{-1}\ s^{-1}$ and $k_2 = 5 \times 10^5\ M^{-1}\ s^{-1}$, as shown by the comparison of the theoretical cyclic voltammograms on the right side of Fig. 5. Importantly, the reliability of these computed values of k_1 and k_2 is further shown in Fig. 6 by the excellent fit of all the simulated cyclic voltammograms to the experimental ones which were obtained by systematically varying the concentrations of PPh_3 and Mn(NCMe) over a rather wide range.

We conclude from the CV simulation studies that the overall rate of electron transfer, including both homogeneous and heterogeneous components in eqs. 16 and 17, is fast compared to the rate of the ligand exchange step in eq. 15. As such, we now inquire about the nature of the rate-limiting exchange step itself since there are two important possibilities, viz., an associative or a dissociative mechanism.

In the digital simulation of the cyclic voltammograms, the ligand exchange reaction in eq. 15 has been implicitly formulated as a one-step, bimolecular substitution reaction. The kinetics of this associative process is given by the second-order rate expression:

$$-\frac{d[MnL^+]}{dt} = k_1[MnL^+][N]$$

The dissociative counterpart to this mechanism is represented as the two-step process below:

$$MnL^+ \underset{k_{-3}}{\overset{k_3}{\rightleftharpoons}} Mn^+ + L$$

$$Mn^+ + N \xrightarrow{k_4} MnN^+ \qquad (20)$$

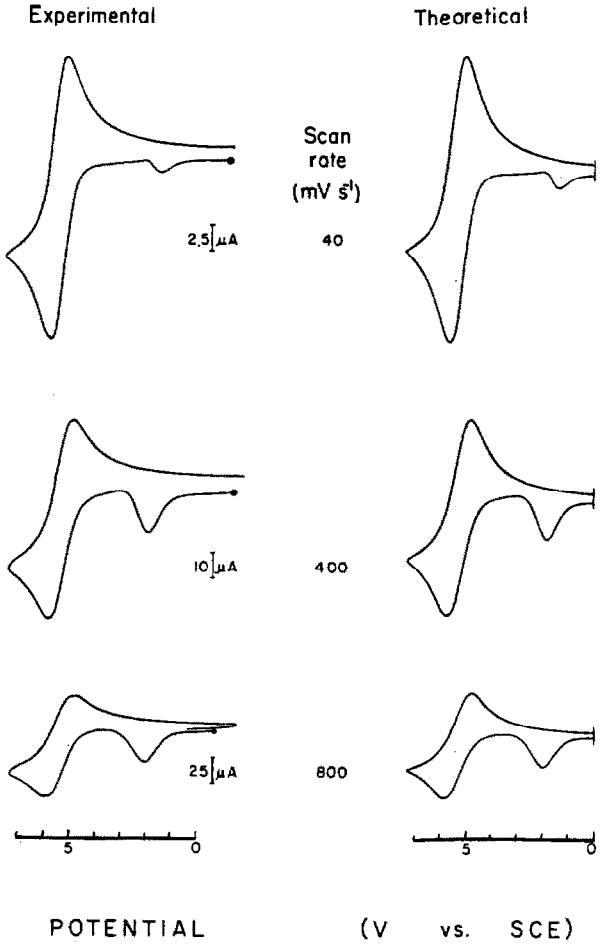

Fig. 5. Computer simulation of the cyclic voltammograms of a solution containing 1.04×10^{-3} *M* Mn(NCMe) and 2.94×10^{-3} *M* PPh_3 in acetonitrile containing 0.1 *M* TEAP at the various scan rates indicated.

For this dissociative mechanism, the general rate expression employing the steady state approximation is given as:

$$-\frac{d[MnL^+]}{dt} = \frac{k_3k_4[MnL^+][N]}{k_{-3}[L]+k_4[N]} \tag{21}$$

for which two limiting kinetic extremes can be considered. First, for a rate-determining dissociation of the ligand L, i.e., $k_{-3}[L] \ll k_4[N]$, the first-order rate expression is independent of nucleophile N. This kinetic description is clearly not compatible with the results in Fig. 6, which shows a marked dependence on PPh_3. Second the other kinetic extreme of $k_{-3}[L] \gg k_4[N]$ is described by the second-order rate expression:

$$\frac{d[MnL^+]}{dt} = \frac{k_3k_4[MnL^+][N]}{k_{-3}[L]} \tag{22}$$

The rate of such a reversible dissociative process is only distinguished from the associative process by an inverse dependence on the concentration of the departing ligand L.

As effective as the computer simulation of the cyclic voltammogram is for the determination of the rate constant k_1, it requires large amounts of computer time for the true iterative optimization of each system. Therefore we considered an alternative approach which stems from the conclusion that there is only one rate-limiting step in the electrocatalytic ligand substitution process. Since the CV wave of the reactant MnL is very sensitive to changes in the concentration of MnL and **N**, as well as the scan rate, we can employ Saveants' a-dimensional analysis [15] of the electrochemical kinetics to express these variables in terms of a single parameter $\lambda = k_1(RT/Fv)[\mathbf{N}]$ where R, T and F have their usual significance. In order to utilize this procedure, we consider the change in the anodic peak current of MnL with and without **N**. This current ratio i_p/i_p° is computed numerically as a function of log λ in order to construct a working curve. Similarly an experimental current ratio i_p/i_p° is plotted against the closely related function $\log(RT/Fv)[\mathbf{N}]$ from the CV data at various scan rates, reactant and nucleophile concentrations. The amount of translation of the working curve relative to the experimental curve therefore represents the value of the rate constant $\log k_1$. Indeed the concurrence of the experimental parameters to afford a unique value of this rate constant provides another compelling confirmation of the validity of the electrochemical kinetics in Scheme 2 to describe the electrocatalytic ligand substitution.

The successful evaluation of the rapid rates of ligand exchange enabled us to determine the structural effects of the substituting nucleophile **N** and of the displaced ligand L on the exchange rate constant k_1 for the cationic MnL^+. It is noteworthy that the second-order rate constants k_1 span a range of more than 10^4 M^{-1} s^{-1} with only minor changes in L and **N**. The second-order rate constans k_1 for the ligand substitution of the 17-electron manganese carbonyl cations are unusual for several reasons. First, the absolute magnitudes of the rate constants are much larger than those commonly encountered in their diamagnetic counterparts. Second, the sensitivity of the rate constant to the structural effects of the incoming nucleophile **N** is unusually high. For example, PPh_3 is more than 10^3 times as reactive as $P(OPh)_3$, whereas in other systems the factor is usually much less. Moreover, the trend in the reactivity of a triad of related triarylphosphine nucleophiles, (viz., triphenylphosphine, tri-*p*-tolylphosphine, and tri-*p*-chlorophenylphosphine) toward ligand substitution of $Mn(NCMe)^+$ coincides closely to that trend observed in the nucleophilic substitution of benzyl chloride. (Note the latter represents a classical example of a bimolecular S_N2 substitution.) Such structural effects on the rate are much more attenuated in other systems. The lability of the leaving ligand is also highly magnified in MnL^+, as shown by the factor of $\sim 10^3$ which separates L = MeCN from L = pyridine, when PPh_3 is the nucleophile in an acetone medium. A thorough analysis of the kinetics data for a series of *p*-substituted pyridine derivatives $Mn(py)^+$ with phosphine nucleophiles leads to the generalized expression:

$$\log k_1 = 17 - 0.15[pK_a^L] + 0.28[pK_a^N] - 0.12[\theta] \qquad (23)$$

which describes (a) the electronic effect of the departing pyridine ligands relative to their Brønsted base strengths $[pK_a^L]$, (b) the electronic effect of the entering phos-

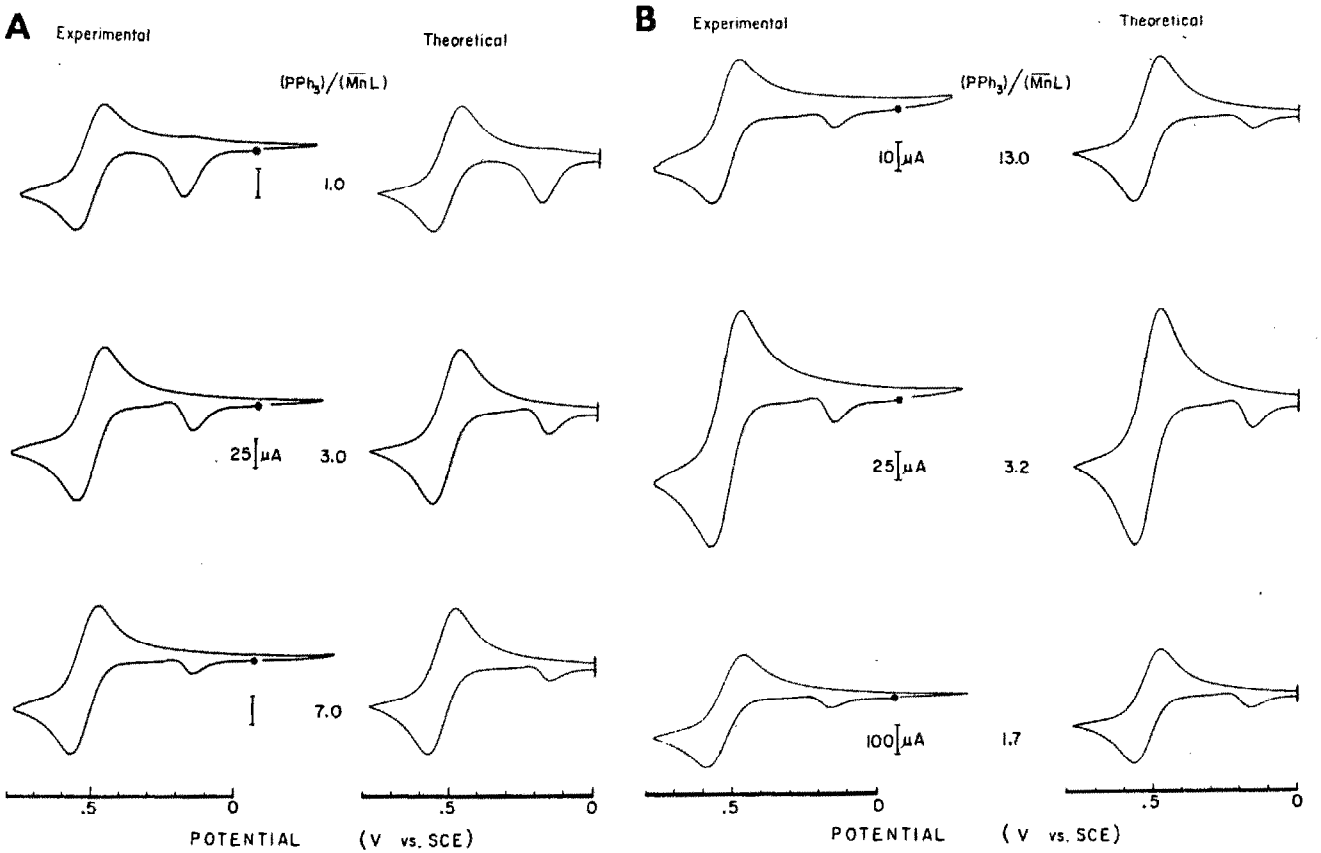

Fig. 6. Agreement between the computed and the experimental CV using the same single set of parameters in Fig. 5. (a) 1.7×10^{-3} *M* Mn(NCMe) with varying molar ratios of PPh_3, as indicated; (b) 1.0×10^{-2} *M* PPh_3 and varying molar ratios of Mn(NCMe), as indicated. All CVs recorded in acetonitrile containing 0.1 *M* TEAP at 22°C and a scan rate of 400 mV s^{-1}.

phine nucleophiles with Brønsted base strengths [pK_a^N], and (c) the steric effects of the phosphine nucleophile as determined by the cone angle [θ] [16]. Finally, it must be emphasized that the associative process dominates the ligand substitution in MnL^+, and any contribution from a dissociative process is minor. The associative mechanism for the ligand exchange step in eq. 18 is also favored by an analysis of the activation parameters. The experimental data consisted of a series of cyclic voltammograms recorded at temperatures varying incrementally from -40 to 25°C. The remarkably linear Arrhenius plot of the exchange rate constant ($\log k_1$) afforded the activation parameters: $\Delta H^{\ddagger}$ 4.4 kcal mol^{-1} and $\Delta S^{\ddagger}$ -25 eu. Indeed, the negative entropy of activation readily accords with the associative mechanism proposed for the ligand exchange process.

In the foregoing, we showed how the kinetics of each step in the catalytic cycle for ligand substitution can be determined. Let us now consider how the thermodynamic driving force for each step in the radical chain process can be measured. We begin by noting that the cyclic voltammogram of Mn(py) in acetonitrile consists mainly of a reversible wave due to the substitution product Mn(NCMe), together with only a minor wave of Mn(py). The reverse process is also observed, albeit less dramatically, in the CV oxidation of Mn(NCMe) in acetonitrile solution containing pyridine (10% v) by the exaggerated separation of the anodic (E_p^{ox}) and cathodic (E_p^{red}) waves. These observations lead to the conclusion that ligand exchange in eq. 24 proceeds readily in both directions, i.e.:

$$\mathrm{Mn(py)} + \mathrm{MeCN} \underset{[E]}{\overset{K_{eq}}{\rightleftharpoons}} \mathrm{Mn(NCMe)} + \mathrm{py} \tag{24}$$

The equilibrium condition in eq. 24 is evaluated quantitatively by the electrostimulation of an acetone solution of Mn(py) and acetonitrile, followed by the quantitative analysis of Mn(NCMe) and Mn(py) by IR spectrophotometry. Similarly, the microscopic reverse process is examined by the electrostimulation of Mn(NCMe) in the presence of various amounts of pyridine and acetonitrile. (In each case, the current efficiencies of the catalytic ligand exchange as measured by coulometry always exceed 20.) The equilibrium constant of $K_{eq} = 1.1 \pm 0.1 \times 10^{-2}$, was found to be independent of the initial conditions, and it corresponds to an overall free energy change of ΔG 2.6 kcal mol^{-1} for eq. 24.

The electron transfer step in the catalytic cycle is given by eq. 25 for which

$$\mathrm{Mn(NCMe)^+} + \mathrm{Mn(py)} \rightleftharpoons \mathrm{Mn(NCMe)} + \mathrm{Mn(py)^+} \tag{25}$$

the free energy change may be evaluated from the formal reduction potentials $E°$ of $Mn(NCMe)^+$ and $Mn(py)^+$. The values of $E°$ are well approximated by the reversible CV peak potentials (i.e., $E° \cong (E_p^{ox} + E_p^{red})/2$), which are listed in Table 2.

Accordingly, we proceed from the Nernstian relationship to calculate the driving force for the electron transfer step in eq. 25 to be -0.19 kcal mol^{-1}. Since the ligand exchange step in eq. 26 simply represents the algebraic difference of the equilibria in eqs. 24 and 25, it follows that the free energy change for the exchange step in eq. 26 is 2.8 kcal mol^{-1}.

$$\mathrm{Mn(py)^+} + \mathrm{MeCN} \rightleftharpoons \mathrm{Mn(NCMe)^+} + \mathrm{py} \tag{26}$$

In the foregoing example, the thermodynamics for the overall ligand substitution

in eq. 24 is largely determined by the driving force for the cation exchange in eq. 26, since the electron transfer step in eq. 25 is close to being isoergonic. Moreover, the facile substitution of the nitrogen-centered ligands by phosphines cited in Table 1 derives from catalytic cycles in which both steps are quite exergonic. Let us now consider the substitution of Mn(norbornene) by acetonitrile in which the electron transfer step (eq. 27) is endergonic (ΔG 5.72 kcal mol^{-1}). Cyclic voltammetry

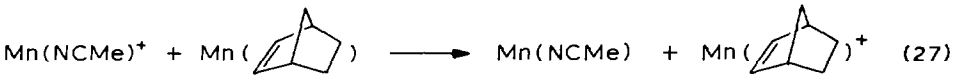

(27)

indicates that the ligand exchange step does occur in the cation (eq. 28), since the

(28)

reversible CV wave of Mn(NCMe) is readily observed on the return sweep from the anodic oxidation of Mn(norbornene) in acetonitrile. Furthermore, it can be demonstrated independently that the equilibrium for the overall ligand substitution process in eq. 29 lies to the right.

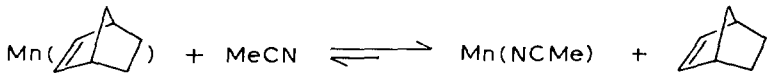

(29)

Nonetheless, the electroxidation of an acetonitrile solution of Mn(norbornene) resulted in only a 21% conversion and a 15% yield of Mn(NCMe), with an overall current efficiency of 2. Under these circumstances, the inefficiency of the electrocatalytic ligand substitution is most simply attributed to the endergonicity of the electron transfer step in eq. 27.

Ligand substitution of polynuclear clusters

Electron transfer catalysis (ETC) of nucleophilic substitution in mononuclear metal carbonyls, as presented above, also applies to their polynuclear counterparts [17]. The difference between ligand substitution by ETC and that by the usual thermal process is nicely illustrated by the behavior of the triiron cluster $Fe_3(\mu_3\text{-}PPh)_2(CO)_9$. Thus following the initial synthesis, Treichel and co-workers found that it underwent ligand substitution with trimethyl phosphite (N) (eq. 30) upon refluxing

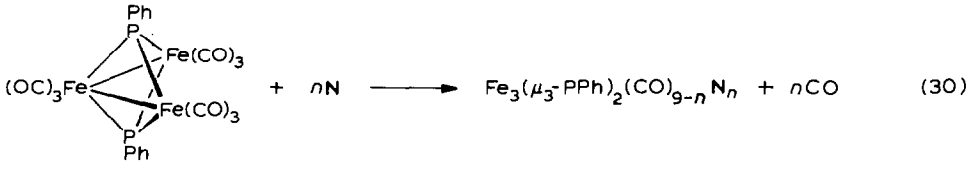

(30)

a xylene solution for $5\frac{1}{2}$ h [18]. A mixture of mono-, di-, and tri-substitution products ($n = 1, 2, 3$ in eq. 30) in approximately equimolar amounts was isolated in low yields. We find that each substitution product can be separately synthesized at room temperature in good yields by simply passing a small cathodic current through the solution at a constant potential E_p until 5–10% charge is consumed [19]. Pure mono-substitution product II ($n = 1$) is isolated in 65% yield when E_p −0.80 V vs.

TABLE 3

ELECTROCATALYTIC SYNTHESIS OF TRIIRON CARBONYL DERIVATIVES [a]

Reactant	Solvent	Ligand	E_p (V)	Electron consumed [b,c]	Product (% Yield) [c]
$Fe_3(PPh)_2(CO)_9$	THF	$P(OMe)_3$	−0.80	0.05	$Fe_3(PPh)_2(CO)_8[P(OMe)_3]$ (65)
$Fe_3(PPh)_2(CO)_9$	THF	$P(OMe)_3$	−0.80 −1.15	0.1 0.1	$Fe_3(PPh)_2(CO)_7[P(OMe)_3]_2$ (63)
$Fe_3(PPh)_2(CO)_9$	CH_3CN	$P(OMe)_3$	−0.80 −1.15	0.1 0.1	$Fe_3(PPh)_2(CO)_7[P(OMe)_3]_2$ (62)
$Fe_3(PPh)_2(CO)_7[P(OMe)_3]_2$	CH_3CN	$P(OMe)_3$	−1.40	1	$Fe_3(PPh)_2(CO)_6[P(OMe)_3]_3$ (39)
$Fe_3(PPh)_2(CO)_9$	THF	PEt_3	−0.80	0.1	$Fe_3(PPh)_2(CO)_8(PEt_3)$ (66)
$Fe_3(PPh)_2(CO)_9$	CH_3CN	PEt_3	−0.80 −1.15	0.1 0.1	$Fe_3(PPh)_2(CO)_7(PEt_3)_2$ (58)

[a] With triiron cluster (0.3 mmol) in 25 ml solvent containing ligand (17 mmol) and Bu_4NClO_4 (0.3 *M*). [b] Total charge passed. [c] Relative to the triiron carbonyl reactant.

SCE. Pure disubstitution product ($n = 2$) is isolated in 63% yield when the charge is

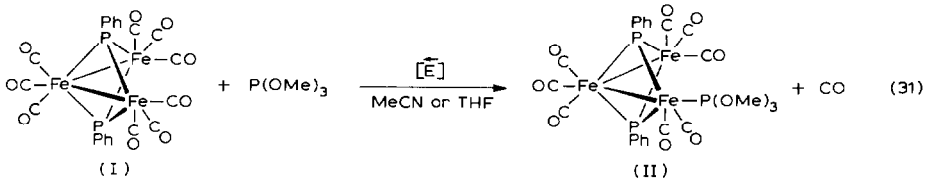

first passed at E_p −0.80 V and then at −1.15 V. Pure trisubstitution product ($n = 3$) is isolated at E_p −1.40 V under the conditions described in Table 3.

The potential E_p determines the selectivity in ligand substitution by selecting the particular triiron carbonyl to be reduced to its radical anion. For example, the cyclic voltammogram of the triiron cluster shows a 1-electron reversible wave with $E°$ −0.79 V which is the potential required for the ligand substitution in eq. 31 (vide supra).

The ESR investigation of the reactive intermediates in ETC ligand substitution of polynuclear metal carbonyls such as the triiron cluster I has provided unusual insight into cluster substitution. Crucial to the success of electrocatalysis is the substitutional lability of the anion radical $I^{\cdot}$ which can be generated by 1-electron reduction (electrochemically or chemically with either sodium amalgam or cobaltocene), to afford a green solution showing the ESR spectrum A in Fig. 7. The triplet splitting (a_p 13.3 G) is readily assigned to the pair of equivalent bridging phenylphosphinidene caps. This initially formed anion radical undergoes a spontaneous rearrangement which destroys the degeneracy of the phosphinidene caps, as shown by the appearance of two doublets in transformed ESR spectrum B. From the difference in the magnitudes of a_p (Table 4), we conclude a geometry change resulting from the cleavage of a Fe–P bond. Indeed the higher *g*-value of this symmetric red-brown species is in agreement with an unpaired electron localized at a

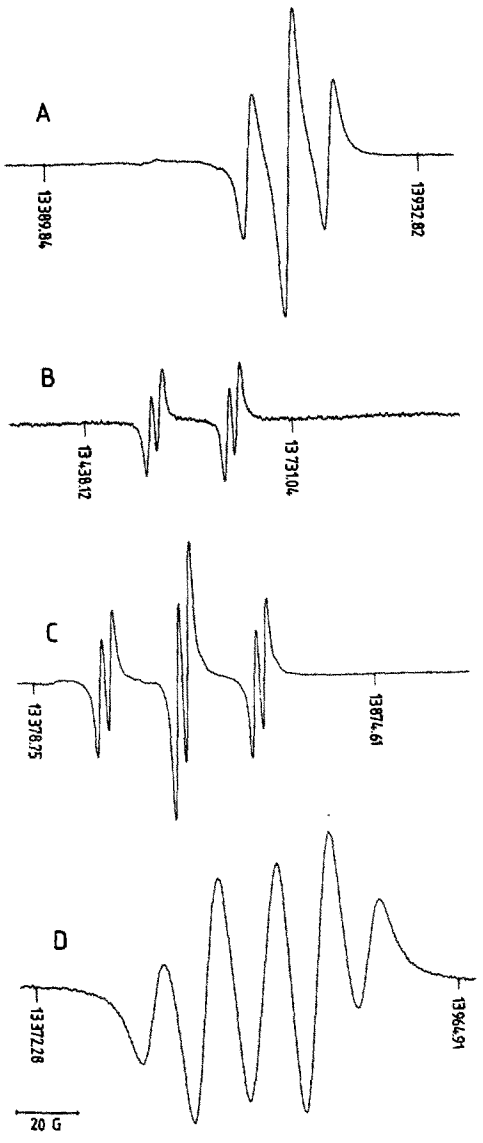

Fig. 7. X-band ESR spectra of anion radicals from (A) reduction of $Fe_3(\mu\text{-}PPh)_2(CO)_9$, (B) A after standing, (C) B upon addition of $P(OMe)_3$ and (D) C after standing or reduction of II followed by $P(OMe)_3$ and standing (solvent, MeCN or THF). NMR field markers are in kHz.

TABLE 4

ELECTROCHEMICAL AND ESR PARAMETERS FOR ANION RADICALS DERIVED FROM $Fe_3(\mu_3\text{-}PPh)_2(CO)_9$

Anion radical	E° [a] (V vs. SCE)	$\langle g \rangle$ [b]	a_p (G)
A. $Fe_3(\mu_3\text{-}PPh)_2(CO)_9^{\mp}$	−0.79	2.019	13.3 (t)
B. $Fe_3(\mu_3\text{-}PPh)(\mu_2\text{-}PPh)(CO)_9^{\mp}$	–	2.039	25.3, 3.4 (d d)
C. $Fe_3(\mu_3\text{-}PPh)(\mu_2\text{-}PPh)(CO)_8L^{\mp}$	–	2.041 [c]	25.3, 25.3, 3.4 (d d d) [d]
D. $Fe_3(\mu_3\text{-}PPh)_2(CO)_8L^{\mp}$	−1.09	2.023 [c]	36.0, 17.8 (d t)

[a] In THF containing 0.3 *M* TBAP. [b] All spectra recorded in THF or MecN at 25°C. [c] L = $P(OMe)_3$. [d] To be consistent with 3 different ^{31}P hfs of similar magnitude observed with L = PEt_3 or PPh_3.

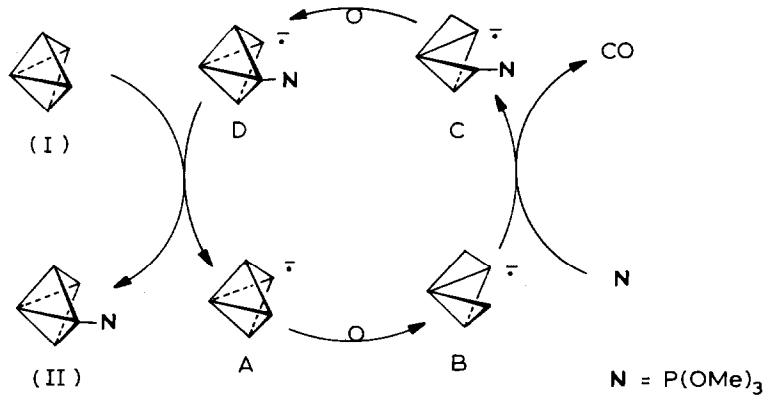

SCHEME 5

17-electron iron center. Reaction of this substitution-labile species with $P(OMe)_3$ immediately leads to an additional splitting in the ESR spectrum C due to the ^{31}P hyperfine coupling of the newly entered ligand. This substituted anion radical then reforms the Fe–P bond to regenerate the parent cluster framework in $II^{\bullet-}$. The latter is demonstrated by the appearance of the ESR spectrum D which is identical with that obtained from the direct 1-electron reduction of II, i.e., $D = II^{\bullet-}$.

These interesting series of cluster transformations is schematically presented in Scheme 5. Their incorporation into the electrocatalytic mechanism requires that $II^{\bullet-}$ readily undergoes electron transfer to I to initiate a new catalytic cycle with $I^{\bullet-}$. Indeed this conclusion is borne out by an exergonic driving force of 6.9 kcal mol for electron transfer, as evaluated by the difference in the standard oxidation potentials ($E°$ in Table 4).

We can thus successfully observe each step in the catalytic cycle shown in Scheme 5. Most importantly the studies of ETC indicate that the ligand substitution occurs in the labile anion radical by first forming a reactive 17-electron iron center via cleavage of a bond to the bridging cap rather than to a contiguous iron. Such a slippage is central to the function of the μ_3-phosphinidene bridge in modulating the reactivity of the cluster. Indeed this intimate involvement of the capping ligand in the substitutional behavior of the anion radical contrasts sharply with that in neutral diamagnetic systems in which the μ_3-bridges are apparently innocent during reactions of the clusters [20].

Conversion of formylmetal to hydridometal carbonyls

Migratory insertion of carbon monoxide to afford acylmetal carbonyls has been shown to proceed rapidly in a series of 17-electron organoiron radicals [21]. Similarly the difference between the behavior of paramagnetic 17-electron formylmetals and their diamagnetic 18-electron precursors is shown dramatically in the formyldirhenate complex *cis*-$(OC)_5ReRe(CO)_4CHO^-$ (III). Thus the formyldirhenate complex III is stable, remaining unchanged in either tetrahydrofuran or acetonitrile solution (typically 10^{-1} M) for several days at 25°C. However, the addition of only

10 mol% of the radical initiator azo-bis(isobutyronitrile) (AIBN) induced the transformation of III to the corresponding hydride IV, i.e.:

$$\underset{\text{(III)}}{(OC)_5ReRe(CO)_4CHO^-} \xrightarrow{[AIBN]} \underset{\text{(IV)}}{(OC)_5ReRe(CO)_4H^-} + CO \qquad (32)$$

in 90% yield within 4 h, at 25°C [22]. The apparent halflife of the formyldirhenate complex III is only 45 min in acetonitrile and 180 min in THF. A turnover number of > 500 is calculated from the known rate of AIBN homolysis under these conditions. The radical-chain nature of the AIBN-induced transformation of III to IV is also revealed by the marked increase in the halflife $\tau_{1/2}$ in acetonitrile to more than 5 h by the presence of one equivalent of dihydroanthracene. The photochemically induced transformation of the formyldirhenate III to the corresponding hydridodirhenate IV also proceeds via a radical-chain pathway. Thus the irradiation of 0.1 *M* III in tetrahydrofuran with light either at λ 400 ± 5 mm using an interference filter or at $\lambda > 400$ nm using sharp cut-off filters affords the hydridodirhenate (eq. 33) in 75% yield with $\tau_{1/2} \sim 30$ min. Importantly this value is

$$(OC)_5ReRe(CO)_4CHO^- \xrightarrow{h\nu} (OC)_5ReRe(CO)_4H^- + CO \qquad (33)$$

markedly increased to $\tau_{1/2} \gg 10$ h in the presence of 1 equiv. of dihydroanthracene. By the use of ferrioxalate actinometry, the quantum yield for the photoinitiated conversion of III of IV is found to be $\phi > 400$. The electronic absorption spectrum of formyldirhenate III has an absorption band at λ_{max} 310 nm and a weak absorption at λ_{max} 400 nm. Previous studies of the parent dirhenium decacarbonyl and its derivatives have shown that the lowest excited states in these complexes are reactive, and lead to homolytic Re–Re cleavage [23] (eq. 34).

$$(OC)_5ReRe(CO)_4CHO^- \xrightarrow{h\nu} Re(CO)_5^{\cdot} + Re(CO)_4CHO^{\cdot-} \qquad (34)$$

Rhenium carbonyl radicals can also be generated electrochemically. For example the galvanostatic reduction [$\bar{E}$] of the formyldirhenate III (2.0×10^{-2} *M*) in acetonitrile containing 0.1 *M* tetraethylammonium perchlorate (TEAP) as the supporting electrolyte consumes 0.035 F of charge per mol of III to yield essentially quantitative yields of the hydridodirhenate IV with the turnover number ≅ 30 (eq. 35). The rapidity of the electrocatalytic process is revealed in the cyclic voltammo-

$$(OC)_5ReRe(CO)_4CHO^- \xrightarrow{[\bar{E}]} (OC)_5ReRe(CO)_4H^- + CO \qquad (35)$$

gram showing the cathodic current for the irreversible wave at E_p −2.1 V to be only one-fifth of that expected for a one-electron reduction. It is accompanied by the simultaneous appearance of the hydridodirhenate IV shown by the CV wave at E_p −2.6 V which is established by comparison with that of an authentic sample. The occurrence of a chain process for decomposition is also evident by the enhancement of the cathodic current for III (and concomitant decrease in IV) by incremental additions of dihydroanthracene. Addition of larger amounts of dihydroanthracene led to a saturation effect, and the cathodic current for the CV wave of III attained a maximum value which was only 60% of that expected from a one-electron reduction. The formyldirhenate III is also found to undergo chain decomposition to its hydride IV in the presence of small amounts of rather strong reducing agents [e]. For

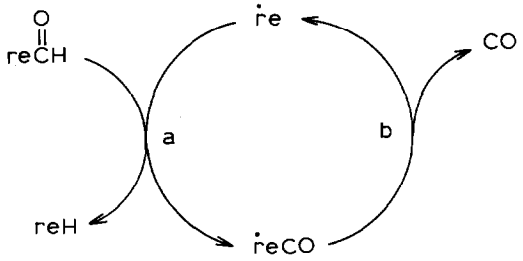

SCHEME 6

example, the addition of sodium anthracene (5 mol%) to a 0.1 *M* solution of III in tetrahydrofuran is sufficient to effect conversion to IV in 75% yield within 10 min at 25°C (eq. 36).

$$(OC)_5ReRe(CO)_4CHO^- \xrightarrow{[e]} (OC)_5ReRe(CO)_4H^- + CO \qquad (36)$$

The long kinetic chain lengths together with the rate retardation by dihydroanthracene indicate an efficient conversion of III to IV by a radical chain process, the propagation sequence of which can be described as shown in Scheme 6 where re = $(OC)_5ReRe(CO)_4^-$. Precedent for both steps of the catalytic cycle derives from the studies of Brown and coworkers [24], who demonstrated the ability of 17-electron carbonylrhenium radicals (i) to abstract hydrogen atoms from various donors as in step a and (ii) to exhibit the substitutional lability of carbonyl ligands as in step b.

Of the four methods of initiation described above, there exists a reasonable correspondence between two of them, namely the thermal (AIBN) and photochemical processes for the conversion of the formyldirhenate III into the corresponding hydride IV. Thus both methods involve comparable turnover numbers of about > 300, and retardation of the same magnitude by dihydroanthracene. Initiation of the chain process by hydrogen atom abstraction from the formylmetal complex is the common factor (eq. 37).

$$In^{\cdot} + (OC)_5ReRe(CO)_4CHO^- \rightarrow In{-}H + (OC)_5ReRe(CO)_5^{\cdot -} \qquad (37)$$

Initiation of the radical chain by AIBN homolysis affords $In^{\cdot} = (CH_3)_2\dot{C}CN$, which is capable of hydrogen atom abstraction of formyl hydrogens, as in eq. 37. Similarly the photolysis of dirhenium carbonyls such as that described in eq. 34 generates mononuclear rhenium carbonyl radicals particularly $Re(CO)_5^{\cdot}$ which can also act as $In^{\cdot}$ in eq. 37.

By contrast, the electrochemical initiation of the chain process is less efficient, the turnover numbers dropping to ~ 30 in the homogeneous experiments and to less than 4–5 in the transient experiments. The marked contrast between the efficiencies of the radical initiation and the electrochemical initiation can be attributed to the reductive instability of the chain carriers $reCO^{\cdot}$ and $re^{\cdot}$ in Scheme 6. In particular, these rhenium carbonyl radicals are subject to further reduction to diamagnetic products, e.g.

$$re^{\cdot} \xrightarrow{e} re^- \xrightarrow{H^+} reH \qquad (38)$$

and/or

$$reCO^{\cdot} \xrightarrow{e} reCO^{-}, \text{ etc.} \tag{39}$$

which effectively interrupt the catalytic cycle. In other words, the electrochemical or reductive methods initiate the chain but simultaneously inhibit it. The overall result would lead to turnover numbers less than those obtained under non-reductive conditions. Such an explanation is supported by the observation that dihydroanthracene is a less effective retarder in electrochemical methods compared to its effect on photochemical and thermal initiation. A detailed analysis of CV peak current on the concentration CO of III and the scan rate v leads to the catalytic mechanism in Scheme 7 to account for the alternative chain process involved in the conversion of III to IV under reductive conditions.

Initiation: $$reCHO + e \rightarrow reCHO^{\cdot -} \tag{40}$$

Propagation: $$reCHO^{\cdot -} \xrightarrow{k_1} reH^{\cdot -} + CO \tag{41}$$

$$reH^{\cdot -} + reCHO \xrightarrow{k_2} reH + reCHO^{\cdot -} \tag{42}$$

SCHEME 7

where $re = (OC)_5ReRe(CO)_4^{-}$. According to Scheme 7, the initiation involves the reduction of III to its dianion radical $reCHO^{\cdot -}$. The extrusion of CO from this 19-electron intermediate may involved one or more steps, but the exact sequence cannot be deduced from the data on hand. On the basis of the dependence on c_0 and v, the pair of deactivating steps described above are attributed to the further evolution of the 19-electron intermediates $reCHO^{\cdot -}$ and $reH^{\cdot -}$. These are associated with extrusion step (eq. 41) and the electron-transfer step (eq. 42), respectively. The electron-transfer mechanism based on Scheme 7 predicts a maximum turnover number of $\backsim 8$ for the catalytic conversion of III to IV. This value compares with the corresponding turnover number of > 300 for the photochemical or thermal activation of the chain. Thus the electron-transfer propagation (Scheme 7) will play a negligible role compared to the radical chain propagation (Scheme 6) unless the latter is inhibited by processes such as those described in eqs. 38 and 39. Furthermore the experimental turnover number for electrochemical activation of 25–30 is significantly higher than that (8) predicted on the basis of Scheme 7 alone. This indicates that the radical-chain propagation (Scheme 6) is also initiated under reductive conditions. Such a reductive initiation relates to the cleavage previously observed with the parent dirhenium decacarbonyl, viz.:

$$Re_2(CO)_{10} \xrightarrow{e} Re(CO)_5^{-} + Re(CO)_5^{\cdot} \tag{43}$$

The analogous cleavage of the Re–Re bond in III leads to rhenium carbonyl radicals, i.e.:

$$(OC)_5ReRe(CO)_4CHO^{-} \xrightarrow{e} \{Re(CO)_5^{\cdot} + Re(CO)_4CHO^{2-}\}$$

$$\text{or } \{Re(CO)_5^{-} + Re(CO)_4CHO^{\cdot -}\} \tag{44}$$

which like In$^{\cdot}$ can enter the catalytic cycle in Scheme 6. Such a reduction can occur

heterogeneously at an electrode surface or homogeneously by reducing agents such as sodium anthracene.

Transient electrochemical techniques have revealed two principal pathways by which the formyldirhenate III undergoes a catalytic chain decomposition. Since the functional transformation of a formyl group to a hydride ligand as in eq. 32 also characterizes the decomposition of many other formylmetal species [25], we inquire whether the same type of radical-chain mechanism outlined in Scheme 6 is a common factor in the apparent instabilities of this general class of organometallic intermediates. We initially focus our attention on the efficient radical chain process under non-reducing conditions which is outlined in Scheme 8, where MCHO and MH are generic representations of the formyl- and hydrido-metal species in the radical chain process:

$$MCHO + \cdot M \rightarrow \cdot MCO + MH \quad (45)$$

$$\cdot MCO \rightarrow CO + \cdot M, \text{ etc.} \quad (46)$$

SCHEME 8

Accordingly we employ a variety of agents (i.e., retarders) in an attempt to intercept the chain-propagating radicals, and thus prolong the halflife (stability) of the formylmetal complexes.

We first examine the stabilization of the formylchromium complex $Cr(CO)_5CHO^-$ since it can be readily generated in $> 70\%$ yield from chromium hexacarbonyl and a slight stoichiometric excess (10%) of potassium triisopropoxyborohydride K(i-PrO)$_3$BH in tetrahydrofuran (THF) solution [26]. Formed under these conditions, it decomposes with an apparent halflife of 39 min at 25°C to afford the hydride $Cr(CO)_5H^-$ and the μ-hydride $(OC)_5CrHCr(CO)_5^-$ in 10 and 17% yields, respectively, among other unidentified products. However the halflife of $Cr(CO)_5CHO^-$ increases sharply in the presence of additives such as γ-terpinene, methoxy-1,4-cyclohexadiene and dihydroanthracene. Moreover, analysis of the decomposition products showed that the yield of the hydride $Cr(CO)_5H^-$ increased with increasing amounts of retarder. (By contrast, the formation of the μ-hydride $(OC)_5CrHCr(CO)_5^-$ is singularly inhibited by the presence of these retarders.) Thus the conversion of the formylchromium complex $Cr(CO)_5CHO^-$ to the corresponding hydride species $Cr(CO)_5H^-$ is consistent with the radical-chain mechanism outlined in Scheme 8. However, such a homolytic pathway cannot be the sole route by which the formyl complex decomposes for two reasons. First, the yield of $Cr(CO)_5H^-$ reaches a plateau of $\sim 45\%$ which is independent of the concentration and the structure of the retarder. Second, the halflife of the formylchromium complex also reaches a limiting value beyond which no added retarder has any effect. Indeed the results show that the limiting values of the halflife are more or less the same for all retarders. Thus we deduce that the plateau of $\tau_{1/2} \sim 170$ min represents a limit beyond which there exists only a nonradical-chain pathway for decomposition of the formyl complex.

The effective retarders have been identified as efficient hydrogen atom donors in organic homolytic systems. Accordingly we next turn out attention to the trialkyltin hydrides which are known to be even more efficient as hydrogen atom donors. Indeed we find that the maximum stabilization (i.e., $\tau_{1/2} \sim 165$ min) for the formylchromium complex $Cr(CO)_5CHO^-$ is readily attained with less than 0.1 equiv of n-Bu$_3$SnH [27]. Further addition of the tin hydride had no effect on the halflife,

in striking accord with the saturation limit described above. Tributyltin hydride is also effective in the stabilization of a variety of other formylmetal complexes. Thus the formyltungsten complex $W(CO)_5CHO^-$ can be generated in 74% yield, and it has an apparent halflife of 16 min at 25°C to afford the μ-hydride $(OC)_5WHW(CO)_5^-$ as the principal decomposition product. In the presence of n-Bu_3SnH, the halflife of $W(CO)_5CHO^-$ is prolonged substantially, and the principal product is the tungsten hydride $W(CO)_5H^-$. Similarly the halflife of the mixed formylacetylrhenium complex $CH_3CORe(CO)_4CHO^-$ can be increased from 8 min to 78 min in the presence of 2 equiv. of n-Bu_3SnH. Even haloformylrhenium complexes such as $BrRe(CO)_4CHO^-$ which is unstable at room temperature can be stabilized by 2 equiv. n-Bu_3SnH ($\tau_{1/2}$ 130 min at 25°C.) Likewise, the neutral formyl complex $Mn(CO)_3(PPh_3)_2CHO$, which decomposes readily at 0°C, can be seen at room temperature ($\tau_{1/2}$ 30 min) in the presence of 2 equiv. of n-Bu_3SnH.

There are some formylmetal complexes such as $(OC)_5MnMn(CO)_4CHO^-$ and $Mo(CO)_5CHO^-$ whose stabilities are not noticeably affected by the presence of n-Bu_3SnH. Since these formyl complexes do not afford the corresponding hydrides as decomposition products, we tentatively infer that the radical-chain mechanism in Scheme 8 is mainly applicable to those formylmetal complexes which are readily converted to their hydride derivatives.

The existence of additional nonradical-chain pathways by which formylmetals can disappear may in part be related to the electron-transfer mechanism identified by transient electrochemical methods in Scheme 7. If so, the divergent behavior of such formylmetal complexes as $(OC)_5MnMn(CO)_4CHO^-$ and $Mo(CO)_5CHO^-$ (vide supra) may be related to the ease by which they participate in electron-transfer processes. We believe that the contribution of electron transfer and other molecular pathways to the decomposition of the other formylmetal intermediates merits further delineation.

Reduction of metal carbonyls such as $Cr(CO)_6$ and $Fe(CO)_5$ leads to their anion radicals as transient intermediates. These 19-electron species are trapped by hydrogen atom donors to afford the corresponding formylmetal complex [28]. The two-step process is schematically represented in eq. 47. The formylmetal in turn is

$$MCO \xrightarrow{[e]} MCO^{\cdot -} \xrightarrow{[H]} MCHO^- \qquad (47)$$

subject to chain decomposition leading to the corresponding hydridometal (eq. 48).

$$MCHO \rightarrow MH + CO \qquad (48)$$

The detailed study of the formyl- to hydrido-metal conversion with formyldirhenate III demonstrates that it is kinetically controlled, being considerably enhanced under radical (AIBN), photochemical, electrochemical, and reductive conditions. Under radical and photochemical conditions, the lifetime of the formylmetal decreases due to a radical-chain process outlined in Scheme 6, in which the radicals re$^\cdot$ and reCO$^\cdot$ are the effective propagating species. Under electrochemical (cathodic) and reductive (sodium anthracene) conditions, these radicals are destroyed (eqs. 38 and 39), which results in the inhibition of the radical-chain process as shown by a decrease in the catalytic turnover numbers from > 300 found in the radical and photochemical activations to 7–30 under reductive conditions. The formyl- to hydrido-metal conversion, which is shown to be also activated under

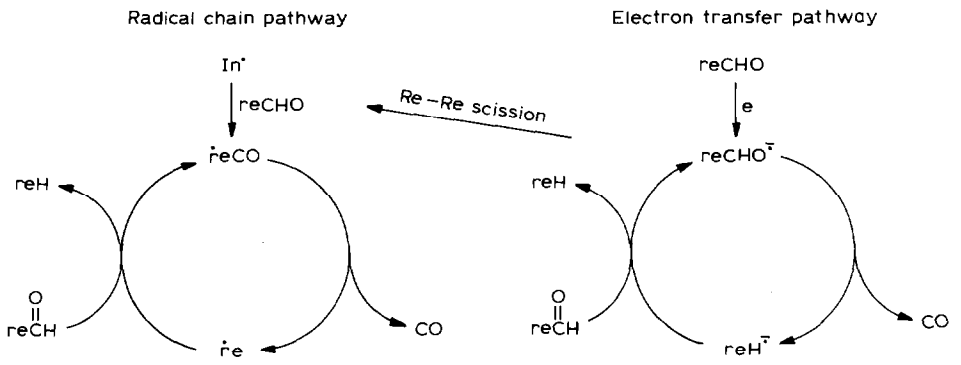

SCHEME 9

reducing conditions, is attributed to the participation of a second catalytic process which is modulated by electron transfer (Scheme 7). In the case of formyldimetals such as $(OC)_5ReRe(CO)_4CHO^-$ III, the two processes are coupled as outlined in Scheme 9 [29].

The generality of the radical-chain process is demonstrated by the unusual stabilization by various hydrogen atom donors of a wide variety of otherwise transient formylmetal species. These hydrogen atom donors act by scavenging the effective propagating radicals in Scheme 8. Thus hydrogen atom transfer in eq. 45 and its microscopic reverse in eq. 47 play a critical role in the production and decomposition of the formylmetal intermediate during the reduction of metal carbonyls.

Acknowledgment

I thank Robert J. Klingler who started us on this odyssey and James W. Hershberger, Christian Amatore, Bikshandarkoil A. Narayanan, Paul M. Zizelman, Michael G. Richmond and Holger H. Ohst for their creative efforts to establish the experimental basis for these ideas. We thank the National Science Foundation and the Robert A. Welch Foundation for the financial support.

References

1 Compare for example, A. Streitwieser, Jr. and C.H. Heathcock, Introduction to Organic Chemistry, 3rd edit., Macmillan, New York, 1985, with K.F. Purcell and J.C. Kotz, Inorganic Chemistry, Sanders, Philadelphia, 1977.
2 C.A. Tolman, Chem. Soc. Rev., 1 (1972) 337.
3 See for example, J.P. Collman and L.S. Hegedus, Principles and Applications of Organotransition Metal Chemistry, University Science Books, Mill Valley California, 1980; C.M. Lukehart, Fundamental Transition Metal Organometallic Chemistry, Brooks/Cole Pub., Monterey, California, 1985; C. Masters, Homogeneous Transition-metal Catalysis, Chapman and Hall, London, 1981; G.W. Parshall, Homogeneous Catalysis, Wiley, New York, 1980.
4 L. Michaelis and M. Schubert, Chem. Revs., 22 (1938) 437. For a historical summary, see R. Stewart, Oxidation Mechanisms. Application to Organic Chemistry, Benjamin, New York, 1964.
5 J.K. Kochi, Organometallic Mechanisms and Catalysis, Academic Press, New York, 1978.
6 F. Basolo and R.G. Pearson, Mechanisms of Inorganic Reactions, 2nd edit. Wiley, New York, 1967. L.H. Langford and H.B. Gray, Ligand Substitution Processes, Benjamin, New York, 1965.

7 G.J. Bezems, P.H. Rieger, S. Visco, J. Chem. Soc. Chem. Commun., (1981) 265.
8 J.W. Hershberger, R.J. Klingler, J.K. Kochi, J. Am. Chem. Soc., 104 (1982) 3034.
9 D.P. Summers, J.C. Luong, M.S. Wrighton, J. Am. Chem. Soc., 103 (1981) 5238.
10 J.W. Hershberger and J.K. Kochi, J. Chem. Soc. Chem. Commun., (1982) 213.
11 I. Wender, P. Pino, (Eds.), Organic Synthesis via Metal Carbonyls, Vol 1, Wiley, New York, 1968. p. 139 and R.S. Nyholm, S.S. Sandhu, M.H.B. Stiddard, J. Chem. Soc., (1963) 5917.
12 J.W. Hershberger, R.J. Klingler and J.K. Kochi, J. Am. Chem. Soc., 105 (1983) 61.
13 J.W Hershberger and J.K. Kochi, Polyhedron, 2 (1983) 929.
14 S.W. Feldberg, J. Phys. Chem., 75 (1971) 2377; S.W. Feldberg and L. Jeftic, ibid., 76 (1972) 2439.
15 J.M. Saveant and E. Vianello, Electrochim. Acta, 8 (1963) 905.
16 P.M. Zizelman, C. Amatore and J.K. Kochi, J. Am. Chem. Soc., 106 (1984) 3771.
17 M.G. Richmond and J.K. Kochi, Inorg. Chem., in press.
18 P.M. Treichel, W.K. Dean, and W.M. Douglas, Inorg. Chem., 11 (1972) 1609. See also J.K. Kouba, E.L. Muetterties, M.R. Thompson, V.W. Day, Organometallics, 2 (1983) 1065.
19 H.H. Ohst and J.K. Kochi, submitted for publication.
20 (a) G. Huttner, J. Schneider, H.D. Müller, G. Mohr, J. von Seyerl, L. Wohlfarth, Angew. Chem., 91 (1979) 82; (b) J. Schneider, G. Huttner, Chem. Ber., 116 (1983) 917; (c) H. Vahrenkamp, Adv. Organomet. Chem., 22 (1983) 169.
21 R.J. Klingler and J.K. Kochi, J. Organomet. Chem., 202 (1980) 49.
22 B.A. Narayanan, C. Amatore, C.P. Casey and J.K. Kochi, J. Am. Chem. Soc., 105 (1983) 6351.
23 See for example, G.L. Geoffroy and M.S. Wrighton, Organometallic Photochemistry, Academic Press, New York, 1979, p. 89f.
24 cf. H.W Walker, G.B. Rattinger, R.L. Belford and T.L. Brown Organometallics, 2 (1983) 775 and ref. cited therein.
25 (a) G.H. Olivé and S. Olivé, Angew. Chem., Int. Ed. Engl., 15 (1976) 136; (b) E.L. Muetterties and J. Stein, Chem. Rev., 79 (1979) 479; (c) C. Masters, Adv. Organometal. Chem., 17 (1979) 61; (d) D.R. Fahey, J. Am. Chem. Soc., 103 (1981) 136; (e) C.P. Casey, S.M. Neumann, M.A. Andrews and D.R. McAlister, Pure Appl. Chem., 52 (1980) 625; (f) R.C. Brady III and R. Pettit, J. Am. Chem. Soc., 103 (1981) 1287; (g) For a review see: J.A. Gladysz, Adv. Organometal. Chem., 20 (1982) 1.
26 C.P. Casey and S.M. Neumann, J. Am. Chem. Soc., 98 (1976) 5395.
27 B.A. Narayanan, C. Amatore and J.K. Kochi, Organometallics, 3 (1984) 802.
28 B.A. Narayanan and J.K. Kochi, J. Organomet. Chem., 272 (1984) C49.
29 B.A. Narayanan, C. Amatore and J.K. Kochi, Organometallics, in press.